**Supplementary Information**

# Study of the pore structure and size effects on the electrochemical capacitor behaviors of porous carbon/quinone derivative hybrids

*Hiroyuki Itoi,*[*][†] *Shuka Tazawa,*[†] *Hideyuki Hasegawa,*[†] *Yuichiro Tanabe,*[†] *Hiroyuki Iwata*[‡] *and*

*Yoshimi Ohzawa*[†]

[†]Department of Applied Chemistry, and [‡]Department of Electrical and Electronics Engineering,

Aichi Institute of Technology, Yachigusa 1247, Yakusa-cho, Toyota, 470-0392, Japan.

*E-mail: itoi-hiroyuki@aitech.ac.jp

**1. Dependence of the saturation amounts on the total pore volumes of the porous carbons.**

Fig. S1 shows the dependence of the saturation amounts of DCBQ on the total pore volumes of the porous carbons used in this study. Note that the saturation amounts are plotted as the weight of the adsorbed DCBQ per gram of the porous carbon ($g_{-DCBQ} \, g_{-PC}^{-1}$). The resulting saturation amounts have the same correlation as the weight of the adsorbed DCBQ per unit electrode volume, as indicated in Fig. 5. Obviously, there is a proportional correlation between the saturation amounts of DCBQ and the total pore volumes of the porous carbons. On the other hand, the saturation amounts have no correlation with the mesopore volumes nor the micropore volumes of the porous carbons. These results indicate that the saturation amounts depend on the total pore volumes of the porous carbons used in this study.
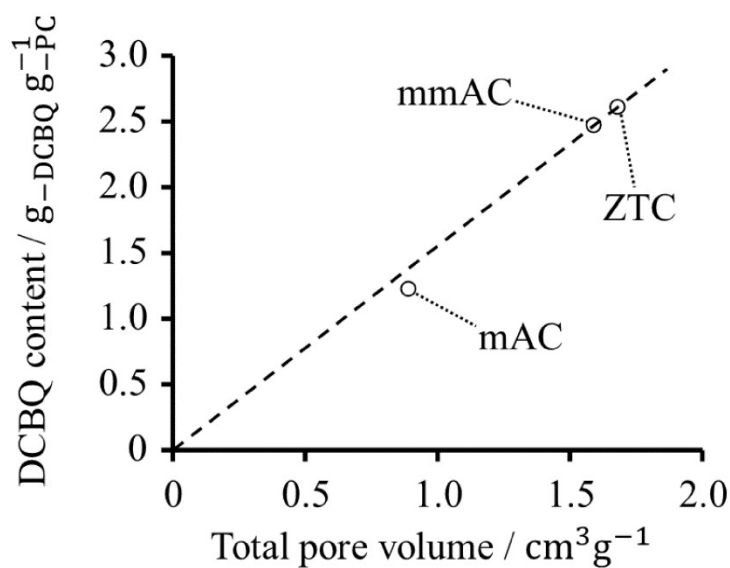


Fig. S1 Dependence of the saturation amounts of DCBQ per gram of the porous carbons used in this study on their total pore volumes.

## 2. Results of the electrochemical capacitor behaviors of porous carbon/DCBQ hybrids plotted based on the weight of active materials.

Fig. S2 shows the results of CV and galvanostatic charge/discharge cycling plotted as the values per gram of the active materials (*i.e.*, the porous carbon and DCBQ). The tendencies of the enhancement in the currents and capacitances of the porous carbon/DCBQ hybrids in the figures are quite different from those in Fig. 6.
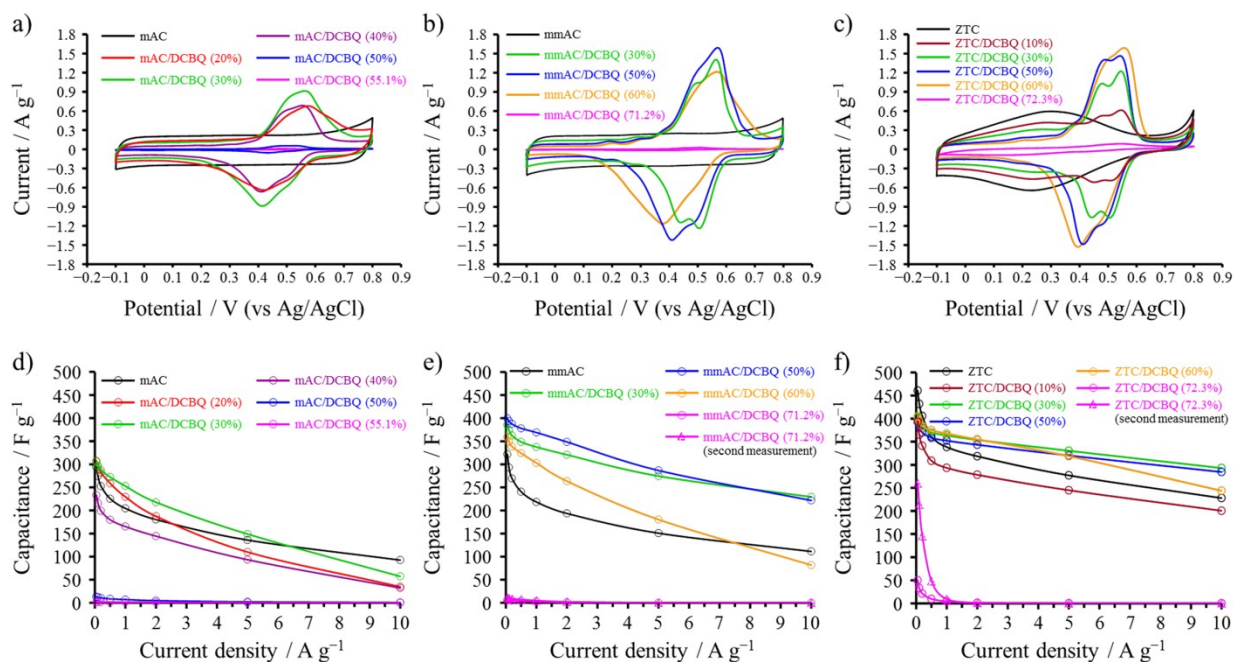


Fig. S2 Results of the electrochemical behaviors of the porous carbon/DCBQ hybrids and pristine porous carbons. (a−c) Cyclic voltammograms of the (a) mAC/DCBQ, (b) mmAC/DCBQ, and (c) ZTC/DCBQ hybrids, respectively, measured at a sweep rate of 1 mV s$^{-1}$. The 4th cycle is plotted for each sample. (d−f) Dependence of the gravimetric capacitances on the current densities for the (a) mAC/DCBQ, (b) mmAC/DCBQ, and ZTC/DCBQ hybrids, respectively. The currents and capacitances in (a−f) are the values based on the mass of active materials. The second measurements of mmAC/DCBQ (71.2%) and mmAC/DCBQ (72.3%) in (e,f) were performed a week after the first measurement.

## 3. Electrochemical measurement of the pristine DCBQ.

We performed the CV measurement of the pristine DCBQ to compare with the electrochemical behaviors of the porous carbon/DCBQ hybrids. For the electrode preparation from the pristine DCBQ, 100 mg of DCBQ was pressed at 200 MPa into a pellet with a diameter of 13 mm. For the electrochemical measurement, a three-electrode stainless steel cell was used because the pellet is fragile and cannot be sandwiched by stainless steel mesh like the electrode sheets of the porous carbon/DCBQ hybrids. The DCBQ pellet was placed in a three-electrode stainless steel cell, together with an aqueous 1 M $H_2SO_4$ electrolyte solution. A counter electrode (13 mm circle) was prepared from mmAC by mixing with PTFE and carbon black (for details, see the Experimental Section in the manuscript).

As shown in Fig. S3, the cyclic voltammogram of DCBQ did not show any redox characteristics in the voltammogram. Since DCBQ is insoluble in aqueous electrolyte solutions and has poor electrical conductivity, little DCBQ molecules undergo redox reaction. This result validates the present hybridization method.
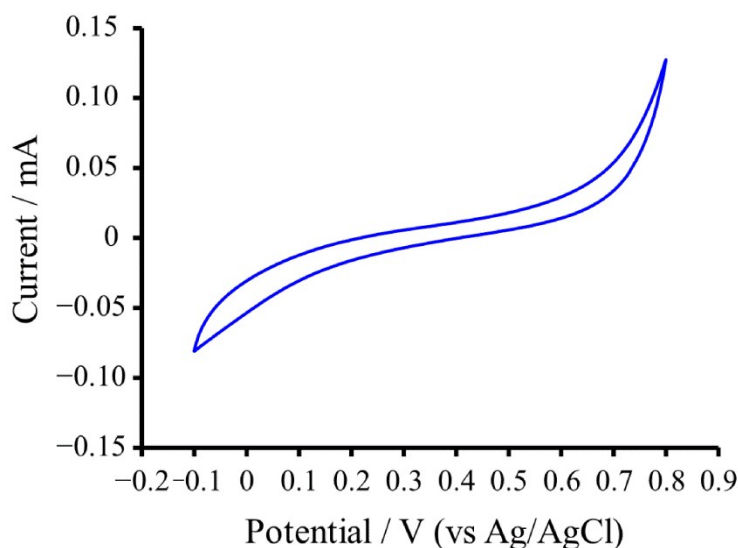


Fig. S3 Result of the CV for the pristine DCBQ measured in an aqueous 1 M $H_2SO_4$ at a sweep rate of 1 mV s$^{-1}$ in the potential range of −0.1 to 0.8 V (25 ºC).

## 4. Calculation of the utilization ratios of DCBQ.

Fig. S4a,b show the typical voltammograms of the AC/DCBQ hybrids (*i.e.*, the mAC/DCBQ and mmAC/DCBQ hybrids) and the ZTC/DCBQ hybrids, respectively. Since mAC and mmAC show a constant electric double-layer current (Fig. 6a,b), the electric double-layer and DCBQ-derived currents are resolved into individual currents, as shown in Fig. S4a. Subsequently, the DCBQ-derived current is integrated, and the utilization ratio was calculated based on the two-electron redox reaction of DCBQ, as shown in the inset of Fig. 7b. On the other hand, the current of the ZTC/DCBQ hybrids in the voltammograms consists of not only the electric double-layer and DCBQ-derived currents but also the current of the quinone groups introduced in the edge sites of ZTC (Fig. S5a), as discussed in the manuscript.[1] The current excluding the quinone group-derived current for the ZTC/DCBQ hybrids can be calculated as shown in Fig. S4b. Since the sum of the double-layer current and the current derived from the quinone groups of ZTC decreases with increasing DCBQ contents due to the disturbance of both the electric double-layer formation and the oxidation of ZTC (Fig. S5b), the base line for subtracting the double-layer- and quinone group-derived currents can be drawn, by simply adjusting the current of the pristine ZTC. As shown in Fig. S4c−f, this method can well estimate the utilization ratios of DCBQ for the ZTC/DCBQ hybrids.
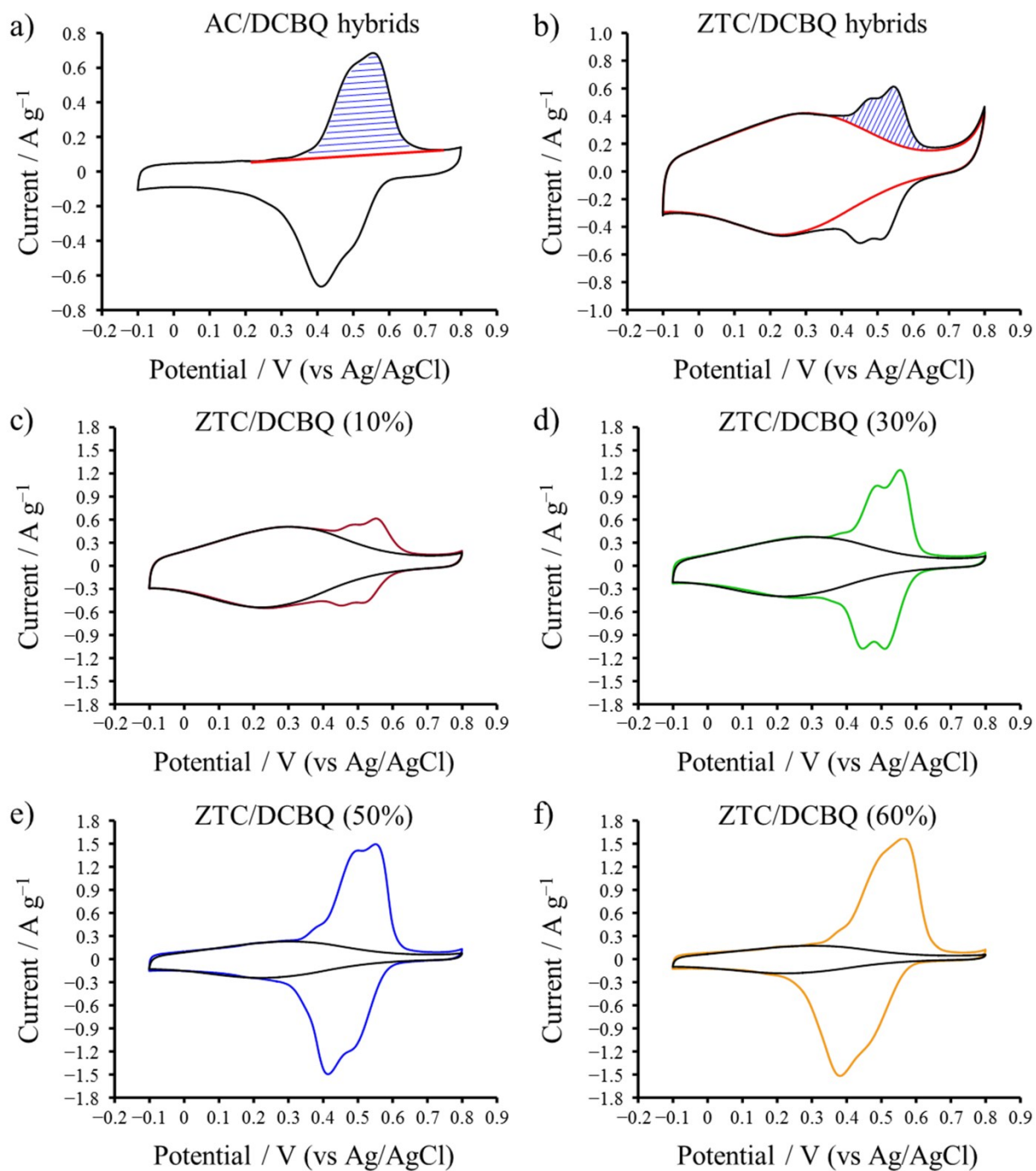
Fig. S4 The calculation method of the utilization ratios for the (a) AC/DCBQ and (b) ZTC/DCBQ hybrids. (c−f) Results of the baseline creation for the ZTC/DCBQ hybrids.

**5. Oxidation of ZTC and ZTC/DCBQ (60%) during the CV measurement.**

Fig. S5 shows the voltammograms of ZTC and ZTC/DCBQ (60%) from the 1st to the 4th cycles. As shown in the voltammograms of ZTC, an irreversible large anodic current is observed above 0.5 V (vs Ag/AgCl) at the first cycle. Subsequently, ZTC shows a broad cathodic current in the reverse sweep (+0.8 V → −0.1 V) and a abroad anodic current in the following sweep (−0.1 V → +0.8 V). The anodic and cathodic currents are reversible and increase with the cycle number, while the irreversible anodic current decreases with the cycle number. These results indicate that the irreversible anodic current is attributed to the oxidation of ZTC, while the reversible peak couple is based on the reversible redox reactions of the quinone groups introduced in ZTC by electrochemical oxidation, thus inducing the pseudocapacitance.[1] On the other hand, the irreversible anodic current of ZTC/DCBQ (60%) is smaller than that of ZTC. Note that the currents in Fig. S5a,b are based on the value per unit volume of the electrode, which contains the same amount of ZTC, as shown in Fig. 5a,d. The reduction in the irreversible anodic current of ZTC/DCBQ (60%) indicates the suppression of the oxidation of ZTC by the adsorbed DCBQ.
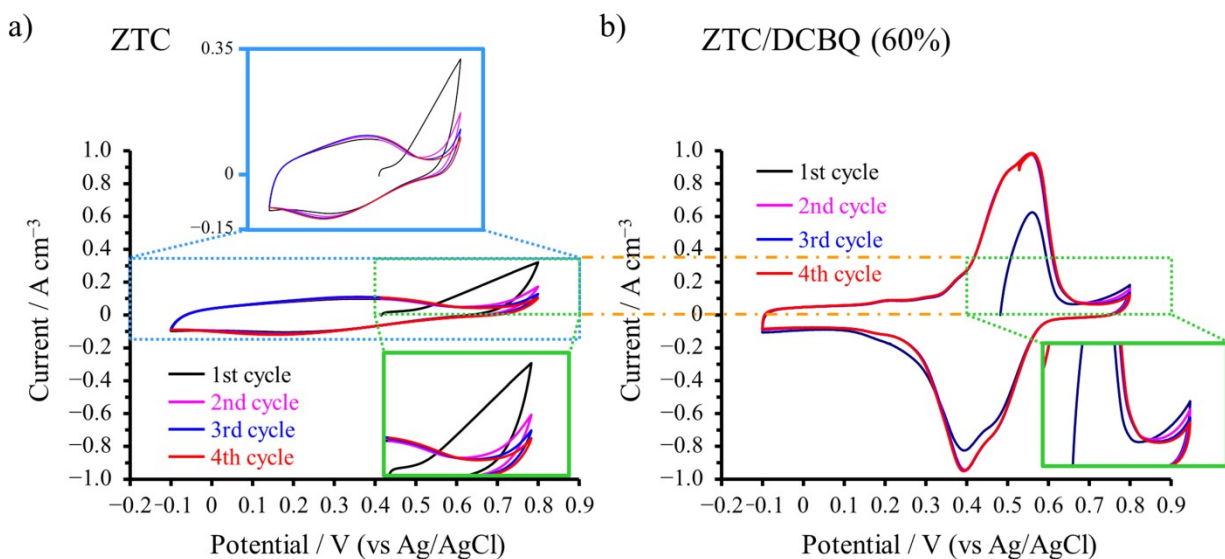


Fig. S5 The voltammograms of (a) ZTC and (b) ZTC/DCBQ (60%). The voltammograms from the 1st to the 4th cycles are plotted.

**6. Results of the electrochemical impedance spectroscopy for the ZTC/DCBQ hybrids.**

Fig. S6 shows the Nyquist plots of ZTC and the ZTC/DCBQ hybrids, obtained by the electrochemical impedance spectroscopy. The measurements were conducted using a three-electrode cell with a potential amplitude of 10 mV at an anodic peak top potential, which was determined from each voltammogram of the ZTC/DCBQ hybrids. The measurement of ZTC was collected at 0.5 V. The charge transfer resistance corresponds to the size of the semicircle in the high-frequency region.[2] ZTC is easily oxidized during CV and introduced by quinone groups (Fig. S5a), and the introduced quinone groups induce the pseudocapacitance, resulting in the increase of the charge transfer resistance.[1] However, the contribution of the quinone groups to the pseudocapacitance is much smaller than that of the adsorbed DCBQ (Fig. 6c). Meanwhile, there is a substantial contribution of the DCBQ-derived pseudocapacitance to the capacitance of the ZTC/DCBQ hybrids; nevertheless, their charge transfer resistances are equal to or smaller than that of the pristine ZTC, except for ZTC/DCBQ (72.3%). Because the charge transfer of DCBQ is facilitated by a large contact area between the conductive carbon surfaces and the adsorbed DCBQ. A large charge transfer resistance of ZTC/DCBQ (72.3%), as shown in the inset of Fig.S6, is explained by the disturbance of the proton conduction within the DCBQ-saturated micropores, which is in agreement with the result of the galvanostatic charge/discharge analysis for ZTC/DCBQ (72.3%) (Fig. 6i).
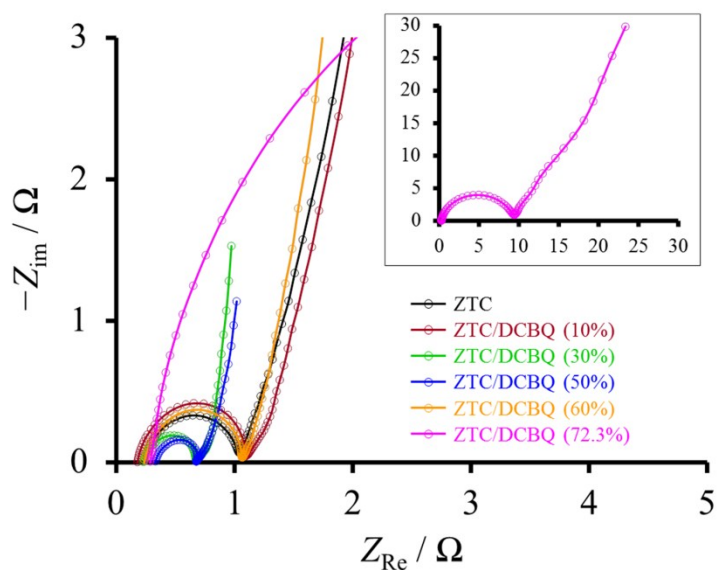


Fig. S6 Nyquist plots of ZTC and the ZTC/DCBQ hybrids.

**7. Effect of the impregnation condition on the electrochemical capacitor performance of ZTC/DCBQ (60%).**

The CV of ZTC/DCBQ (60%) was conducted immediately after the immersion of the electrode of ZTC/DCBQ (60%) into the electrolyte solution, while the counter electrode was fully impregnated by electrolyte solution, as explained in the Experimental Section in the manuscript. As shown in the result of the CV measurement (Fig. S7), the current in the first cycle was very small due to the inadequacy of the electrolyte impregnation. However, the current clearly increased in the following cycle, and the peak top current in the 4th cycle reached the same value as that in Fig S2c, indicating the adequate impregnation. These observations suggest that the electrolyte solution was easily impregnated even in the DCBQ-constrained micropores.
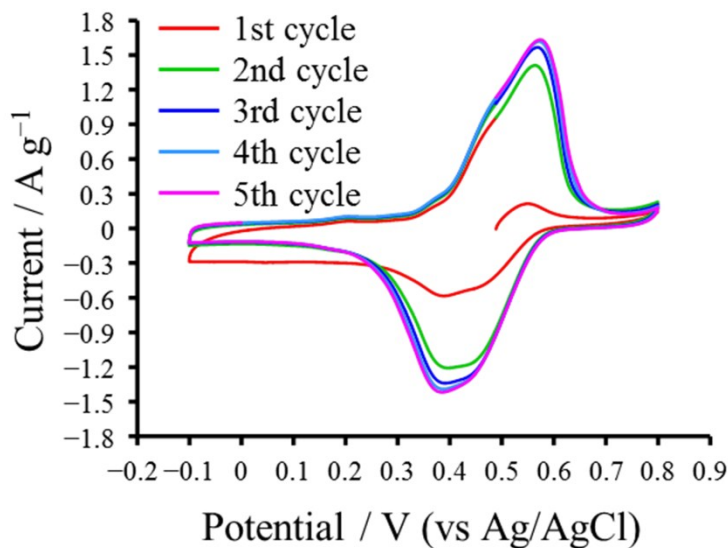


Fig. S7 The result of the CV for ZTC/DCBQ (60%) performed without the electrolyte impregnation procedure. The measurement was performed using a three-electrode cell at a sweep rate of 1 mV s$^{-1}$ in the potential range of −0.1 to 0.8 V.

References

1. Itoi, H.; Nishihara, H.; Ishii, T.; Nueangnoraj, K.; Berenguer-Betrián, R.; Kyotani, T. *Bulletin of the Chemical Society of Japan* **2014**, *87*, 250.
2. Tong, J.; Zhang, H.; Gu, J.; Li, L.; Ma, C.; Zhao, J.; Wang, C. *Journal of Materials Science* **2016**, *51*, 1966.